Poly(ethylene glycol)-Induced Fusion and Destabilization of Human Plasma High-Density Lipoproteins†

Shobini Jayaraman, Donald L. Gantz, and Olga Gursky*

Department of Physiology and Biophysics, Boston University School of Medicine, Boston, Massachusetts 02118

Received December 17, 2003; Revised Manuscript Received March 8, 2004

ABSTRACT: High-density lipoproteins (HDL) are macromolecular complexes of specific proteins and lipids that mediate the removal of cholesterol from peripheral tissues. Chemical unfolding revealed that HDL fusion and rupture are the two main kinetic steps in HDL denaturation. Here we test the hypothesis that lipid fusogens such as poly(ethylene glycol) (PEG) may promote lipoprotein fusion and rupture and thereby destabilize HDL. We analyze thermal disruption of spherical HDL in 0−15% PEG-8000 by calorimetric, spectroscopic, electron microscopic, and light scattering techniques. We demonstrate that the two irreversible high-temperature endothermic HDL transitions involve particle enlargement and show a heating rate dependence characteristic of kinetically controlled reactions with high activation energy. The first calorimetric transition reflects HDL fusion and dissociation of lipid-poor apolipoprotein A-1 (apoA-1), and the second transition reflects HDL rupture and release of the apolar lipid core. Neither transition involves substantial protein unfolding; thus, the transition heat originates from lipid and/or protein dissociation and repacking. At room temperature, PEG-8000 induces HDL fusion that is distinct from the heat-, denaturant-, or enzyme-induced fusion since it leads to formation of larger particles and does not involve apoA-1 dissociation. Increasing the PEG concentration in solution from 0 to 15% leads to low-temperature shifts by approximately −18 °C in the two calorimetric HDL transitions without altering their nature. Thus, consistent with our hypothesis, PEG-8000 induces fusion and reduces the thermal stability of HDL. Our results suggest that PEG is useful for the analysis of the molecular events involved in metabolic HDL remodeling and fusion.

Lipids in the body are transported in the form of plasma lipoproteins that are heterogeneous complexes of lipids and specific proteins termed apolipoproteins (*1*−*3*). HDL,[1] which are the smallest and densest of these complexes (diameter $d = 7.2-12$ nm, density of 1.063−1.21 g/mL), mediate the removal of cholesterol from peripheral tissues to the liver via the process of reverse cholesterol transport (reviewed in refs *1*−*4*). This function of HDL, along with the antioxidant effect of HDL-associated enzymes on the low-density lipoproteins (LDL) (*5*), contributes to the well-established antiatherogenic action of HDL and its major protein, apoA-1 (*6*, *7*).

During their metabolism, HDL undergo extensive remodeling by plasma factors (reviewed in refs *3*, *4*, and *8*). ApoA-1, which is produced in the liver and gut probably as a lipid-free or lipid-poor molecule, acquires phospholipids and cholesterol from the cell membranes via the interaction with the ATP-binding cassette transporter, and is converted to nascent discoidal HDL. These nascent HDL, which contain two to three molecules of apoA-1 wrapped around the phospholipid bilayer disk comprised mainly of phosphatidylcholines (PC) and cholesterol, provide a substrate for lecithin:cholesterol acyltransferase (LCAT). Following the LCAT reaction, the apolar molecules of cholesterol esters (CE) partition between the disk monolayers, leading to the maturation of HDL into spherical particles; such spherical HDL have a hydrophobic core comprised of CE and a small amount of triglycerides (TG), and a polar surface comprised mainly of PC and apolipoproteins. These small HDL (termed HDL_3, $d = 7-8$ nm, two apoA-1 molecules per particle) are further remodeled via the action of LCAT or phospholipid transfer protein (PLTP) into larger particles (HDL_2, $d = 9-12$ nm, three to four apoA-1 molecules per HDL). These and other HDL modifications by LCAT, PLTP, and hepatic lipase have been shown to involve particle fusion and the concomitant release of lipid-poor or lipid-free apoA-1 (*4*, *8*−*14*). HDL fusion has also been proposed to be involved in the modification of HDL by cholesterol ester transfer protein (CETP) that transfers CE among high-, low-, and very low-density lipoproteins (*15*). Moreover, the formation of the HDL subclass containing apoA-1 and the second major HDL protein, apoA-2, is thought to involve particle fusion (*8*, *10*). Thus, several key steps in HDL metabolism critically

† This work was supported by NIH Grant GM67260 to O.G. The CD spectroscopy, calorimetry, electron microscopy, and protein chemistry core facilities are supported by NIH Program Project Grant HL26355 (D. Atkinson, Program Director).

* To whom correspondence should be addressed: Associate Professor of Physiology and Biophysics, Boston University School of Medicine, W329, 715 Albany St., Boston, MA 02118. Phone: (617) 638-7894. Fax: (617) 638-4041. E-mail: Gursky@bu.edu.

[1] Abbreviations: HDL, high-density lipoproteins; LDL, low-density lipoprotein; apoA-1, apolipoprotein A-1; apoA-2, apolipoprotein A-2; LCAT, lecithin:cholesterol acyltransferase; CE, cholesterol ester; TG, triglycerides; CETP, cholesterol ester transfer protein; PLTP, phospholipid transfer protein; PC, phosphatidylcholine; SR-BI, scavenger receptor class B type I; PEG-8000, poly(ethylene glycol) with an M_w of ≅8000; GdmHCl, guanidinium hydrochloride; DSC, differential scanning calorimetry; EM, electron microscopy; CD, circular dichroism.

10.1021/bi036274r CCC: $27.50
Published on Web 04/14/2004

hinge on the enzyme-induced HDL fusion that leads to formation of distinct HDL subclasses with different compositional, structural, and metabolic properties. HDL fusion by plasma enzymes such as CETP, PLTP, or hepatic lipase also leads to a release of monomolecular lipid-poor apoA-1 that is an important primary acceptor of cellular cholesterol and phospholipids (reviewed in ref *11*). The molecular details underlying HDL fusion and apoA-1 dissociation and the factors that promote or inhibit these reactions remain unknown and are in the scope of this work.

Another related aspect of this work is the energetic and structural basis for HDL stability. Our recent studies revealed that discoidal and spherical HDL form a new class of macromolecular assemblies that are stabilized by kinetic barriers (*16*, *17*); we proposed that similar barriers preclude spontaneous interconversions among different HDL subclasses and thereby regulate HDL functions and lifetime in plasma (*17*). Our thermal denaturation studies of model discoidal HDL (*16*, *18*, *19*), supported by the earlier reports (*20*−*22*), showed that the particle stability is determined by kinetic rather than thermodynamic factors. Correlation of the circular dichroism (CD) spectroscopic, light scattering, and electron microscopic (EM) data revealed that (i) the heat-induced apolipoprotein unfolding is coupled to disk fusion and (ii) the transient disruption of lipid and/or protein packing interactions during fusion provides a large enthalpic contribution to the high free energy barrier for disk stability (*16*, *18*, *19*). Similarly, guanidinium hydrochloride (GdmHCl) denaturation studies of mature spherical HDL from human plasma revealed that fusion and rupture are the two main kinetic events in HDL disruption, and showed that these events are associated with high free energy barriers that determine HDL stability [$\Delta G^* = 16-17$ kcal/mol (*17*)]. These results corroborate the earlier observations of the heat- or denaturant-induced HDL enlargement and disruption (*23*, *24*) and explain the slow unfolding of HDL proteins by GdmHCl (*23*, *25*, *26*). They indicate clearly that the kinetic stability of HDL originates from the high-energy transition states that form the bottlenecks of the fusion and rupture reactions. In this work, we explore the factors that may alter these transition states and thereby affect HDL fusion and rupture.

In contrast to the extensively characterized molecular events involved in membrane fusion (for a recent review, see ref *27*), the mechanisms of lipoprotein fusion and rupture remain unclear. Furthermore, the factors that may reduce or increase the free energy of the transition states and thereby promote or inhibit HDL fusion and rupture have not been determined. The aim of this study is to assess the effects of factors such as dehydration on the morphology and thermal stability of HDL. To do so, we utilize a lipid fusogen, poly(ethylene glycol) with a M_w of ≅8000 (PEG-8000), that is widely used to induce cell fusion and to mediate fusion and rupture of model lipid bilayer systems, thereby providing a model for molecular events in secretory, viral, and membrane fusion (*29*−*33*). Although the molecular mechanism of the PEG-mediated bilayer fusion is not fully understood, it is based, in part, on the vesicle dehydration by PEG that facilitates close contact between the vesicles necessary for their fusion (*28*−*31*). Similarly, the use of PEG as a precipitating agent in protein crystallization stems from the dehydration of the protein by PEG. We hypothesize that PEG-8000 at concentrations that induce vesicle aggregation and fusion (5−18%, v/v) may promote HDL fusion and rupture and thereby destabilize HDL without significantly destabilizing the HDL apolipoproteins. To test this hypothesis, we determine the effects of PEG-8000 on the morphology and thermal transitions of HDL.

MATERIALS AND METHODS

Preparation of Lipoproteins and Apolipoproteins. HDL were isolated from the EDTA-treated plasma of healthy volunteer donors (one male and one female) by density gradient ultracentrifugation in the density range of 1.08−1.21 g/mL that includes only spherical HDL (*34*). HDL from different plasma pools of individual donors were prepared and analyzed separately. The sample purity assessed by a combination of size and density agarose gel electrophoresis (that clearly resolves HDL and LDL bands) was 95%; it was confirmed by the electron microscopic analysis of the particle size that showed no significant HDL contamination with the LDL-size particles. An HDL solution with a protein concentration of 12 mg/mL was dialyzed extensively against a buffer solution containing 10 μM sodium phosphate (pH 7.7), 0.25 mM NaEDTA, and 0.02% NaN_3, which is a standard buffer used in this study. The HDL stock was stored in the dark at 4 °C and was used over the course of 4 weeks; no protein or lipid degradation was detected during this period. The stock solution was diluted with buffer containing 0 or 40% (v/v) PEG. The final PEG concentration ranged from 0 to 15% (v/v), and the final protein concentration in HDL samples ranged from 10−40 μg/mL (in fluorescence and far-UV CD experiments) to 3.5−3.8 mg/mL (in DSC, EM, near-UV CD, and light scattering experiments). The pH of all solutions was 7.7.

Human apoA-1, which was isolated and purified from plasma HDL following the protocol of Wetterau and Jonas (*35*), migrated as a single band on SDS−polyacrylamide gels. The protein (98% pure), which was lyophilized and stored at −20 °C, was dissolved to a concentration of 0.1 mg/mL in the buffer containing 8 M urea, 0.05% EDTA, and 0.02% NaN_3 and was refolded by consecutive dialysis against buffer solutions containing 6, 4, and 2 M GdmHCl, followed by extensive dialysis against the denaturant-free buffer. Human apoA-1 prepared by this method has been shown to retain full biological activity (*34*). The folded apoA-1 was concentrated using an Amicon filter to a final protein concentration of ∼4 mg/mL in the stock solution. To prevent oxidation, the protein was refolded, concentrated, and stored in the dark at 4 °C. The stock solution was used within 1 month of the refolding; no changes in the protein conformation or stability were detected during this period.

For physicochemical experiments, the stock apoA-1 solution was diluted with the buffer containing 0 or 40% PEG-8000; the final concentration of lipid-free apoA-1 ranged from 10−40 μg/mL (for far-UV CD and fluorescence) to 1.5−3.5 mg/mL (for near-UV CD), and the final PEG concentration ranged from 0 to 15%. The protein concentration in HDL and in apoA-1 solutions was determined by a modified Lowry assay and was confirmed by UV absorption at 280 nm. All spectroscopic data were independent of the protein concentration in the range explored.

Differential Scanning Calorimetry. The heat capacity $C_p(T)$ of HDL solutions (3.5−3.8 mg/mL protein and 0−15%

PEG) was recorded using an MC-2 differential scanning microcalorimeter (Microcal, Amherst, MA) that was rebuilt and upgraded by the manufacturer. Degassed HDL and buffer solutions of identical PEG concentrations were subjected to a nitrogen pressure of 20 psi. The $C_p(T)$ data were recorded during heating at a rate of 90 °C/h from 10 °C to the maximal temperature of 115 °C, followed by cooling and incubation at 5 °C for 1−6 h before the next scan was recorded. The results were independent of the incubation time between the consecutive scans. The buffer baselines were subtracted. The resulting $C_p(T)$ data showed a positive slope in the pretransitional region that increased with an increase in the PEG concentration; such a slope, which may result from the high viscosity of the PEG-containing HDL solutions, leads to an uncertainty in the baseline determination. This, along with the HDL heterogeneity and the irreversible character of the thermal transitions (described below), precluded the quantitative thermodynamic analysis of the calorimetric data. ORIGIN was used for the data collection, processing, and display. All DSC experiments were repeated three to five times to ensure reproducibility.

Electron Microscopy. HDL solutions (3.5−3.8 mg/mL protein and 0−15% PEG) that were subjected to various thermal treatments were visualized by negative staining electron microscopy as described previously (*16*, *17*). Images were recorded under low-dose conditions in a CM12 transmission electron microscope (Philips Electron Optics). PHOTOSHOP computer graphics with EXCEL were used for the analysis of the particle size distribution; 350−450 particles were used for such an analysis. The accuracy in the determination of the average diameter is ±0.2 nm. All experiments were carried out in triplicate to ensure reproducibility.

Circular Dichroism Spectroscopy and Light Scattering. CD data were recorded using an upgraded AVIV 62-DS spectropolarimeter with a Peltier temperature control. Far-UV CD data (185−250 nm) were recorded from HDL or apoA-1 solutions of 20−40 μg/mL protein placed in 5 mm cells; near-UV CD data (250−320 nm) were recorded from similar solutions of 3.5−3.8 mg/mL protein placed in 5 mm cells. The PEG concentration in HDL and in apoA-1 solutions varied from 0 to 15%. Under these conditions, no significant contribution of PEG to the far- or near-UV CD spectra was detected. The spectra were recorded with a bandwidth of 1 nm, a step size of 1 nm, and an accumulation time per data point of 15 s and averaged over two or three scans. The melting curves were recorded at 222 and 270 nm during sample heating and consecutive cooling from 20 to 98 °C, with a 1 °C increment and an accumulation time per data point of 30 or 300 s, which corresponds to heating and cooling rates of 11 and 80 °C/h, respectively. In far-UV CD, the signal $\Theta_{222}(T)$ at 222 nm (that is proportional to the protein α-helical content) was used to monitor thermal unfolding. In near-UV CD, the largest heat-induced changes in HDL were observed at 270−280 nm; the CD signal at 270 nm, $\Theta_{270}(T)$, was used to monitor these changes, which optimized the signal-to-noise ratio. The buffer baselines were subtracted from the data that were normalized to the protein concentration and were expressed as molar residue ellipticity, [Θ], in far-UV CD, and as molar ellipticity in near-UV CD. ORIGIN was used for the data analysis and display. All CD experiments were repeated three to six times.

In a separate series of experiments, far-UV CD spectra and the melting curves at 222 nm were recorded from concentrated HDL solutions (∼2 mg/mL protein) placed in 0.5 mm cells; comparison with far-UV CD data recorded in similar experiments with dilute HDL solutions (20 μg/mL protein) showed that the lipoprotein concentration has no significant effect on the secondary structure or the apparent transition temperature of HDL.

Heat-induced changes in turbidity were monitored by the dynode voltage $V(T)$ that was recorded simultaneously with the CD melting data $\Theta(T)$ as described previously (*16*). The dynode voltage is proportional to the reduction in the light intensity due to the combined effects of light absorption and scattering. Although $V(T)$ does not significantly change during thermal unfolding of nonaggregating proteins, our studies of model discoidal HDL revealed that it may increase substantially with the heat-induced increase in particle size, reflecting increased light scattering of these particles (*16*). Therefore, measuring the $V(T)$ function in CD experiments is useful for monitoring the heat-induced changes in the size and/or morphology of discoidal HDL (*16*, *18*). Here, we use a similar approach for the analysis of the PEG-containing solutions of spherical HDL. We simultaneously monitor dynode voltage and CD data at 270 nm [$V_{270}(T)$ and $\Theta_{270}(T)$, respectively] upon heating the HDL solution (3.5−3.8 mg/mL protein and 15% PEG) at a rate of 11 or 80 °C/h, and correlate the results with the DSC and EM data recorded of identical HDL samples in similar heating experiments.

Fluorescence Spectroscopy. Intrinsic fluorescence and near-UV CD of HDL are dominated by apoA-1 that comprises 70% of the total HDL protein and contains four Trp and seven Tyr residues (in comparison, apoA-2 comprises 20% of the total HDL protein and has no Trp and four Tyr residues). Emission spectra of apoA-1 and HDL were recorded at 20−99 °C using a FluoroMax-2 spectrofluorimeter with a water bath temperature control. Freshly prepared samples containing filtered buffer and/or protein or lipoprotein (10 μg/mL protein) were placed in a 1 cm quartz cell. The emission spectra were recorded from 315 to 540 nm with 5 nm excitation and emission slit widths. Excitation wavelengths of 280 and 296 nm were used to record the total emission and Trp emission, respectively. In the heating experiments, the temperature of the water bath was increased in 5−10 °C increments, the sample was equilibrated at each temperature, and the spectra were recorded at time intervals that approximate the heating rates of 80−90 °C/h used in our CD and DSC experiments. The baseline correction was applied to all emission spectra. The wavelength of the emission maximum, λ_{em}, was determined at various temperatures with an accuracy of ±2 nm. The results were qualitatively similar regardless of the excitation wavelength used (280 or 296 nm). All experiments were repeated three to five times to ensure reproducibility.

RESULTS

Thermal Transitions in Intact HDL. Figure 1 shows the heat capacity $C_p(T)$ of HDL in PEG-free buffer recorded by DSC upon heating at a rate of 90 °C/h. With direct heating from 10 to 115 °C, a double-peaked endotherm is observed (bottom curve), with the first peak (half-width $\Delta T_{1/2} \sim$ 10 °C) centered at 92 °C and the second sharper peak

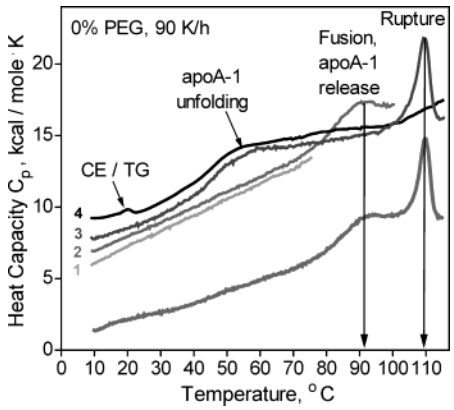

FIGURE 1: Thermal transitions in intact HDL monitored by DSC. The heat capacity $C_p(T)$ was recorded when the HDL solution with a protein concentration of 3.8 mg/mL was heated at a rate of 90 °C/h. The data curves were shifted along the *Y*-axis to avoid overlap. The bottom curve was recorded during direct heating of intact HDL from 5 to 115 °C. The top curves (1−4) show consecutive scans recorded from the same sample upon heating from 5 °C to incrementally increasing temperatures, followed by cooling and incubation at 5 °C: (1) 75, (2) 95, (3) and 115 °C, and (4) next scan to 115 °C. Consecutive scans to 115 °C (curves 5 and 6, not shown) closely overlap with curve 4. Two high-temperature transitions in intact HDL (the first attributed to HDL fusion/apoA-1 dissociation and the second to HDL rupture) are indicated. Thermal transitions in the consecutive scans centered near 58 °C [that is attributed to apoA-1 unfolding (*36*, *37*)] and near 18 °C [that corresponds to the phase transition in CE and TG which are released from ruptured HDL and form large lipid droplets (Figure 2C)] are indicated.

($\Delta T_{1/2} \sim 5$ °C) at 110 °C. The peak positions could be reproduced to 1 °C for HDL samples from the same plasma pool but varied by 2−4 °C for HDL from different pools, possibly reflecting differences in the particle composition. Similar double-peaked endotherms with the variable peak positions were reported earlier (*36*−*38*). The relatively small peak width, especially for the second transition, contrasts with the broad low-cooperativity thermal unfolding of lipid-free apolipoproteins [$\Delta T_{1/2} \sim 30$ °C for apoA-1 (*39*)], suggesting that the calorimetric HDL transitions reflect dissociation and repacking of proteins and/or lipids rather than protein unfolding.

To elucidate the physical origin of the HDL transitions and to test their reversibility, the DSC data were recorded during heating of the same sample from 10 °C to incrementally increasing temperatures that correspond to the onsets and/or conclusions of the two calorimetric peaks, followed by cooling and incubation at 5 °C (curves 1−4 in Figure 1). Heating to 75 °C (the onset of the first DSC peak) does not produce any irreversible heat capacity changes, as indicated by the full superimposition of the first and second scans from 10 to 75 °C (curves 1 and 2). In contrast, heating to 100 °C (conclusion of the first peak and onset of the second peak) completely eliminates the first HDL peak from the next scan (curves 2 and 3 compared), indicating the irreversibility of the first calorimetric transition. Instead, the next scan shows a broad peak centered near 58 °C (curve 3); a similar peak observed in the earlier studies was attributed to the unfolding of apoA-1 that was shown to dissociate from HDL during the first calorimetric transition (*36*, *37*). In addition, curve 3, which extends to 115 °C, shows the second calorimetric peak; the midpoint, shape, and size of this peak are identical to those observed upon direct heating of intact HDL from 10 to 115 °C (Figure 1, bottom curve). Consequently, the first and second calorimetric peaks constitute distinct independent structural transitions in HDL.

The next DSC scan to 115 °C shows a small but significant peak near 20 °C (curve 4); this peak has been attributed to the liquid crystal phase transition in the mixture of CE and TG that are released from the HDL core during the second calorimetric transition (*36*, *37*). This scan also shows the broad peak near 58 °C but no peaks at higher temperatures, indicating irreversibility of the second HDL transition. The amplitude of the 58 °C peak in curves 3 and 4 and in the consecutive scans to 115 °C (curve 5, not shown) remains invariant, suggesting that heating beyond the second calorimetric transition does not lead to any significant changes in the concentration of the dissociated apoA-1. This suggests that apoA-1 dissociates from HDL mainly during the first DSC transition.

To assess the effects of heating on the morphology of HDL and to correlate these effects with the calorimetric transitions, intact HDL were heated at a rate of 80−90 °C/h to incrementally increasing temperatures encompassing the range of the calorimetric transitions, followed by cooling to 22 °C and visualization by negative staining electron microscopy. In intact HDL, more than 80% of particles have diameters from 7.5 to 11 nm, with an average diameter $\langle d \rangle$ of 9.1 nm (Figures 2A and 3A). Heating to 60−70 °C (before the onset of the first DSC peak) does not cause any significant changes in the particle size distribution (data not shown). However, heating to 98 °C (conclusion of the first DSC peak) leads to a substantial increase in the population of the enlarged HDL-like particles ($d = 11-13$ nm) at the expense of the smaller 7−9 nm HDL (Figures 2B and 3B); as a result, the average particle diameter $\langle d \rangle$ increases to 10.1 nm. A similar change in the particle size distribution was detected at room temperature upon incubation of HDL in 2

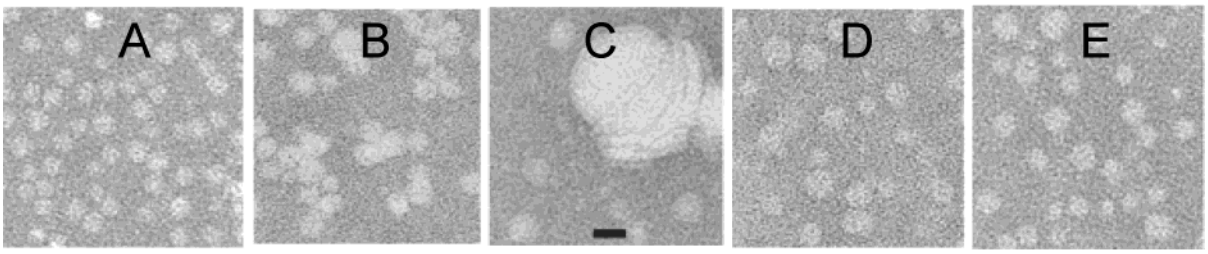

FIGURE 2: Effects of HDL exposure to heat and PEG-8000 on the particle size and morphology. Electron micrographs show negatively stained HDL subjected to various treatments: (A) intact HDL, (B) HDL after heating at 90 °C/h to 98 °C, (C) HDL after heating at 90 °C/h to 115 °C, (D) HDL after overnight incubation at 22 °C in 15% PEG-8000, and (E) same as panel D after extensive dialysis against the PEG-free buffer. The bar is 15 nm long.

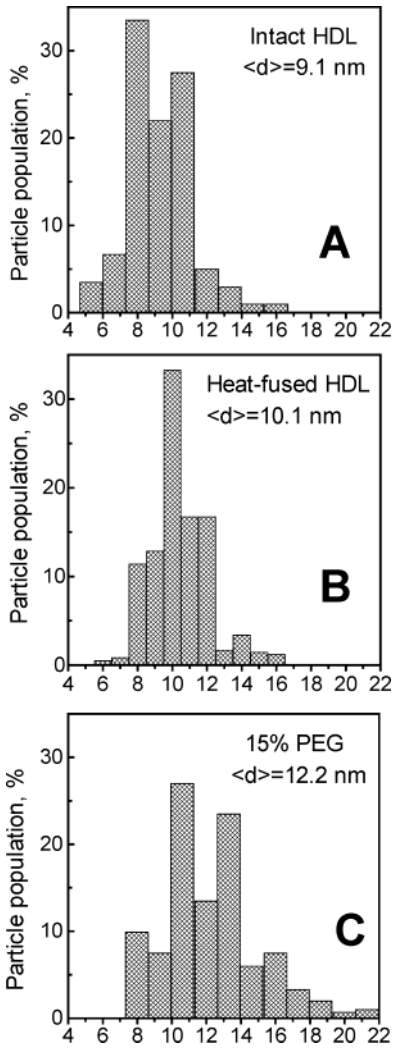

FIGURE 3: Particle size distribution in intact, thermally fused, and PEG-fused HDL: (A) intact HDL (corresponding to Figure 2A), (B) HDL after fast heating to 98 °C (corresponding to Figure 2B), and (C) HDL after overnight incubation at 22 °C in 15% PEG-8000 (corresponding to Figure 2D). The average particle diameters, which were determined with an accuracy of ±0.2 nm, are given.

M GdmHCl (*17*). Consideration of the lipoprotein size and composition suggests that such a change is consistent with fusion of two to three 7−9 nm HDL and formation of one 11−12 nm particle, with a possible release of up to two apoA-1 molecules (*17*). Thus, chemical and thermal denaturation produces similar changes in the particle size distribution that are consistent with HDL fusion.

In addition to the enlarged HDL-like particles, the heating to 115 °C (completion of the second calorimetric transition) results in the formation of large lipid droplets that are remnants of ruptured HDL (Figure 2C). This irreversible rupture is consistent with the CE phase transition near 20 °C detected in the DSC scans recorded after HDL had been heated to 115 °C (Figure 1, curve 4). It is also consistent with the earlier reports of HDL rupture in the second calorimetric transition (*37*, *38*). Moreover, a similar mixture of fused and ruptured particles was observed upon incubation of HDL at 22 °C in relatively high concentrations of GdmHCl (3−6 M) (*17*). This suggests that chemical and thermal denaturation proceed through similar major steps, which are HDL fusion under mild denaturing conditions followed by rupture under stronger denaturing conditions. Correlation of the EM and DSC data in Figures 1 and 2A−C suggests that the first calorimetric peak involves HDL fusion and concomitant apoA-1 dissociation, while the second sharper peak involves particle rupture and release of the apolar lipid core.

Effects of PEG on the Size and Thermal Stability of HDL. To test whether PEG-8000 at concentrations that promote liposome fusion can fuse lipoproteins, HDL were incubated overnight at 22 °C in buffer solutions containing up to 15% PEG and were visualized by EM. Electron micrographs show that, in the presence of 7.5−15% PEG, the particles retain their HDL-like morphology but become significantly enlarged and heterogeneous in size compared to intact HDL (compare panels A and D of Figure 2). The average particle diameter $\langle d \rangle$ in 15% PEG is 12.2 nm, larger than that of the thermally fused HDL ($\langle d \rangle$ = 10.1 nm), and the size distribution is broader, extending beyond 16 nm (Figure 3B,C). Thus, PEG-8000 induces HDL fusion at 22 °C that is distinctly different from the thermal fusion.

The effects of PEG on the thermal stability of HDL were assessed by DSC. HDL samples containing 0, 7.5, and 15% PEG were heated from 5 to 115 °C at a rate 90 °C/h. The $C_p(T)$ data (Figure 4) clearly show that increasing the PEG concentration from 0 to 15% leads to a low-temperature shift in both calorimetric peaks by −18 °C. Similar shifts by −16 to −18 °C were detected in HDL isolated from other plasma pools. Furthermore, in the presence of PEG, the second transition becomes sharper and its half-width $\Delta T_{1/2}$ is reduced from ∼5 °C in 0% PEG to ∼2 °C in 7.5−15% PEG, suggesting an increased cooperativity of this transition.

The PEG-induced changes in the calorimetric transitions depicted in Figure 4 may result from the PEG-induced HDL enlargement at 22 °C (Figure 2D) or from the presence of PEG in solution during heating. To differentiate between these possibilities, HDL solutions were incubated with 15% PEG, followed by extensive dialysis against PEG-free buffer. Electron micrographs of these dialyzed samples showed a significant population of enlarged particles (Figure 2E), indicating incomplete reversibility of the PEG-induced HDL enlargement. DSC data of these dialyzed samples (not shown) resembled those of intact PEG-free HDL (Figure 4, top curve); the half-width of the second peak ($\Delta T_{1/2} \sim 5$ °C) was identical to that observed in PEG-free HDL, and the peak temperature (106 °C) was only 4 °C lower than that in PEG-free HDL (110 °C), yet 14 °C higher than that in 15% PEG (92 °C). Thus, despite substantial differences in particle size in panels A and E of Figure 2, the cooperativity unit involved in the second calorimetric transition is similar and the apparent thermal stability is only slightly reduced for the PEG-enlarged HDL compared to intact HDL. Consequently, the presence of PEG in solution is required for the increased cooperativity of the second calorimetric transition and, to a large extent, for the low-temperature shifts in both transitions.

To test whether the presence of PEG alters the nature of the thermal transitions in HDL, DSC data were recorded upon heating HDL solutions containing 7.5 and 15% PEG at 90 °C/h from 10 °C to incrementally increasing temperatures corresponding to the onsets and/or conclusions of the DSC peaks, followed by cooling and incubation at 5 °C. Thus, HDL in 15% PEG were heated to 70 °C (onset of the first DSC peak; bottom curve in Figure 4), cooled to 5 °C, heated

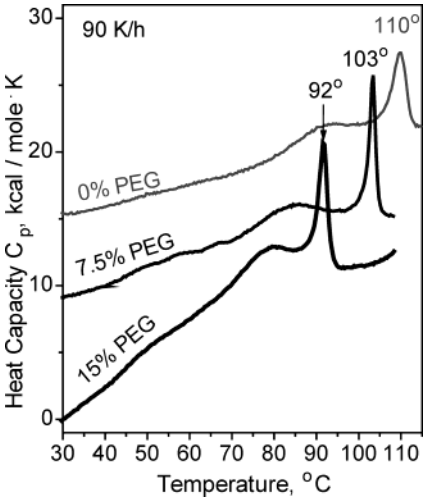

FIGURE 4: Effects of PEG on the calorimetric transitions in HDL. Heat capacity data were recorded upon heating HDL samples containing 0−15% PEG-8000 from 10 to 115 °C at 90 °C/h. The HDL protein concentration is 3.8 mg/mL, and the PEG concentrations are given. The curves are shifted along the *Y*-axis to avoid overlap.

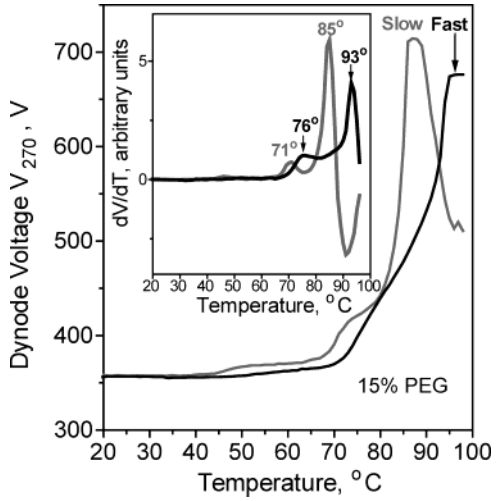

FIGURE 5: Effects of the heating rate on the HDL transitions monitored by turbidity in CD experiments. HDL solutions (3.8 mg/mL protein and 15% PEG) were heated from 20 to 98 °C at a fast (80 °C/h) or slow rate (11 °C/h), and the dynode voltage $V(T)$ was recorded at 270 nm. High turbidity and lipid phase separation exhibited by the heated samples, especially after slow heating, indicate HDL rupture. Loss of sample after rupture explains the high-temperature plateau in the $V(T)$ curves followed by a reduction in $V(T)$ during slow heating. The inset shows first derivatives $dV(T)/dT$ of the dynode voltage melting curves. Arrows denote the peak temperatures in the $dV(T)/dT$ function recorded during fast heating. Comparison with the DSC peak temperatures recorded from an identical sample at a similar heating rate (Figure 4, bottom line) indicates that the two DSC transitions involve an increase in turbidity, i.e., formation of larger particles.

to 85 °C (conclusion of the first and onset of the second peak), cooled to 5 °C, heated to 95 °C (conclusion of the second peak), etc. Comparison of these data (not shown) with the results of similar experiments with intact HDL (Figure 1) shows a clear analogy between the calorimetric transitions in the presence and absence of PEG. Thus, like intact PEG-free HDL, HDL in 15% PEG shows an apoA-1 peak around 58 °C after being heated beyond the first calorimetric transition, and a CE/TG peak near 20 °C after being heated beyond the second calorimetric transition. This indicates clearly that the nature of the two irreversible thermal transitions in HDL is not significantly altered in the presence of PEG; the first calorimetric peak reflects dissociation of apoA-1 from the fused HDL, and the second peak reflects particle disruption and release of the apolar lipid core.

The DSC data in Figure 4 show that the presence of 15% PEG in an HDL solution reduces the temperature of the second calorimetric transition below the boiling point, thereby facilitating the observation of this transition by spectroscopic methods. We took advantage of this observation and used 15% PEG to analyze the structural changes that accompany the two calorimetric HDL transitions. To monitor the heat-induced changes in the particle size, we utilized dynode voltage [$V(T)$] measurements in the CD experiments as outlined in Materials and Methods and in refs *16* and *18*. The conditions for these CD experiments, including sample composition and concentration (3.8 mg/mL HDL protein and 15% PEG) and the heating rate (80 °C/h), closely resemble those of the DSC experiments, thereby facilitating direct correlation of the $C_p(T)$ and $V(T)$ data (black curves in Figures 4 and 5). The dynode voltage $V(T)$ recorded from HDL upon fast heating (80 °C/h) from 20 to 98 °C remains constant up to 70 °C but shows a large biphasic increase from 70 to 95 °C followed by a plateau from 95 to 98 °C. This heat-induced increase in turbidity cannot be reversed upon cooling, suggesting that it reflects an irreversible increase in the particle size due to fusion rather than reversible lipoprotein aggregation. This irreversible increase in turbidity occurs in the same temperature range as the two calorimetric HDL transitions in 15% PEG (70−95 °C), which is evident from the comparison of the peak temperatures in the first derivative of the dynode voltage data, $dV(T)/dT$, with the corresponding $C_p(T)$ peaks (black lines in the inset of Figure 5 and in Figure 4). Consequently, these transitions are accompanied by an irreversible increase in particle size. This heat-induced increase in particle size detected by turbidity is consistent with the heat-induced HDL fusion and rupture observed by EM in the temperature range of the two calorimetric transitions (Figure 2A−C). Thus, the correlation of the turbidity, EM, and DSC data corroborates the notion that the first and second calorimetric peaks involve HDL fusion and rupture, respectively.

To test whether the heat-induced HDL fusion and rupture involve a high activation energy, dynode voltage data [$V_{270}(T)$] were recorded at two heating rates of 80 and 11 °C/h (Figure 5, black and gray lines marked "fast" and "slow", respectively). Comparison of these melting curves clearly shows a low-temperature shift of approximately −8 °C in both thermal transitions when the scan rate is slowed from 80 to 11 °C/h. Such a shift is characteristic of irreversible transitions associated with a high activation energy (*40*). Consequently, like the denaturant-induced HDL fusion and rupture (*17*), the heat-induced HDL fusion and rupture have a high activation energy and thus are subject to kinetic control.

Effects of PEG and Temperature on the HDL Protein Conformation. To test the effects of PEG-8000 on the structure and stability of HDL proteins, CD and fluorescence spectra of the major HDL protein, apoA-1, were recorded in 0−15% PEG. Far- and near-UV CD and intrinsic Trp fluorescence spectra (that report on the protein secondary structure, aromatic packing, and Trp solvent exposure,

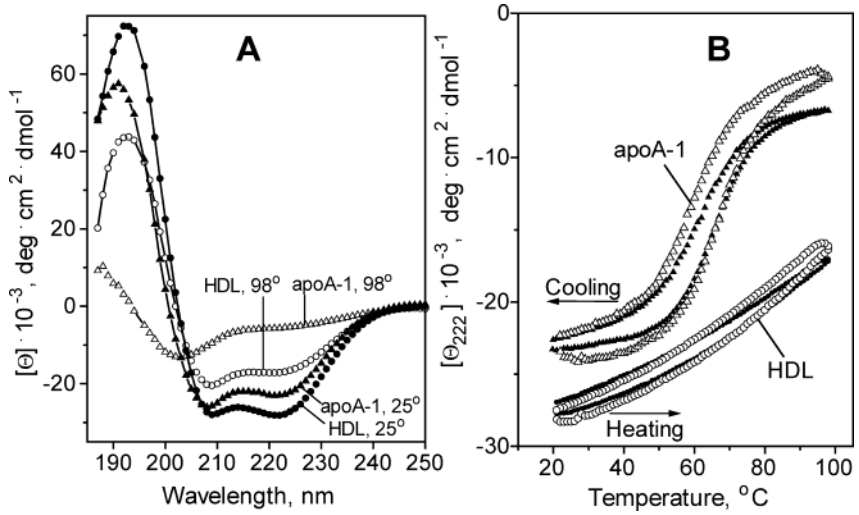

FIGURE 6: Far-UV CD data of HDL and its major protein, lipid-free apoA-I, at various temperatures. The protein concentration is 20−40 μg/mL, and PEG concentrations are 0−15%. The spectra recorded at different PEG concentrations but otherwise identical conditions fully overlap; therefore, only one representative spectrum is shown for each condition. (A) CD spectra of HDL and apoA-1: (▲) apoA-1 at 25 °C, (△) apoA-1 at 98 °C, (●) HDL at 25 °C, and (○) HDL at 98 °C after being heated from 20 to 98 °C at 80 °C/h (such a heating results in HDL fusion in 0% PEG and HDL rupture in 15% PEG). (B) Thermal unfolding and refolding of the helical structure in apoA-1 and HDL monitored at 222 nm upon heating and consecutive cooling from 20 to 98 °C at a rate of 80 °C/h: (▲) apoA-1 in 0% PEG, (△) apoA-1 in 15% PEG, (●) HDL in 0% PEG, and (○) HDL in 15% PEG. The directions of temperature changes are shown.

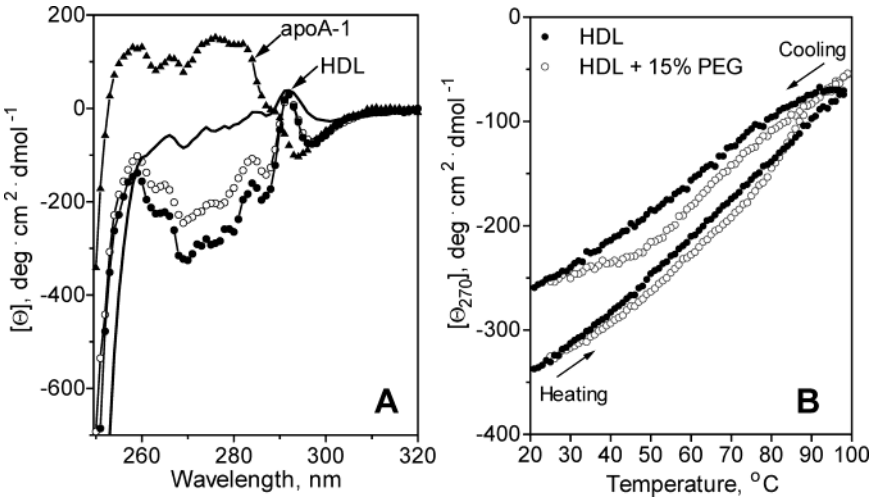

FIGURE 7: Near-UV CD data of HDL and apoA-l at various temperatures. The protein concentration is 3.5−3.8 mg/mL for HDL and 1.5 mg/mL for lipid-free apoA-1, and PEG concentrations are 0−15%. The spectra recorded at different PEG concentrations but otherwise identical conditions fully overlap; therefore, only one spectrum is shown for each condition. (A) CD spectra of HDL and apoA-1: (▲) lipid-free apoA-1 at 25 °C, (●) HDL at 25 °C, (—) HDL at 98 °C after heating at 80 °C/h, and (○) HDL at 25 °C after heating and cooling from 25 to 98 °C at 80 °C/h. (B) Melting curves recorded at 270 nm upon heating and consecutive cooling from 20 to 98 °C: (●) HDL in 0% PEG and (○) HDL in 15% PEG. The directions of temperature changes are shown.

respectively) of lipid-free apoA-1 (triangles in Figures 6A, 7A, and 8A) show no detectable changes upon addition of PEG. Furthermore, the melting curve of free apoA-1 recorded upon heating from 0 to 98 °C by CD at 222 nm (that is proportional to the α-helical protein content) does not significantly change when the PEG concentration is increased from 0 to 15% [Figure 6B (▲ and △)]. Consequently, PEG has no detectable effect on the secondary and tertiary structure or thermal stability of lipid-free apoA-1.

To test whether the heat-induced morphological transitions in HDL observed by DSC, EM, and light scattering (Figures 2−5) are accompanied by protein unfolding, the protein conformation on HDL in 0−15% PEG was monitored in the temperature range from 20 to 98 °C by far- and near-UV CD (Figures 6 and 7) and by Trp fluorescence (Figure 8). Far-UV CD melting curves at 222 nm, $\Theta_{222}(T)$, recorded from HDL solutions containing 0 and 15% PEG [Figure 6B (● and ○)] largely superimpose and are nearly linear; similar nearly linear melting curves were observed in the earlier spectroscopic studies of HDL (*26*, *41*, *42*). In addition, the HDL melting curves recorded in this study are independent of the scan rate in the range explored (11−80 °C/h) and show a close superimposition of the heating and cooling curves (Figure 6B), as well as of the first scan and consecutive scans (not shown). This suggests that HDL heating from 20 to 98 °C is accompanied by a largely reversible noncooperative reduction in protein α-helical content.

Lipid-free apoA-1 is completely unfolded at 98 °C, as indicated by the negative CD band at 203 nm and by the low residual ellipticity at 222 nm [Θ_{222}(98 °C) ≅ −5000 deg cm^2 dmol^{-1}] that is characteristic of fully unfolded helical proteins [Figure 6A (△)]. In contrast, the spectrum of HDL

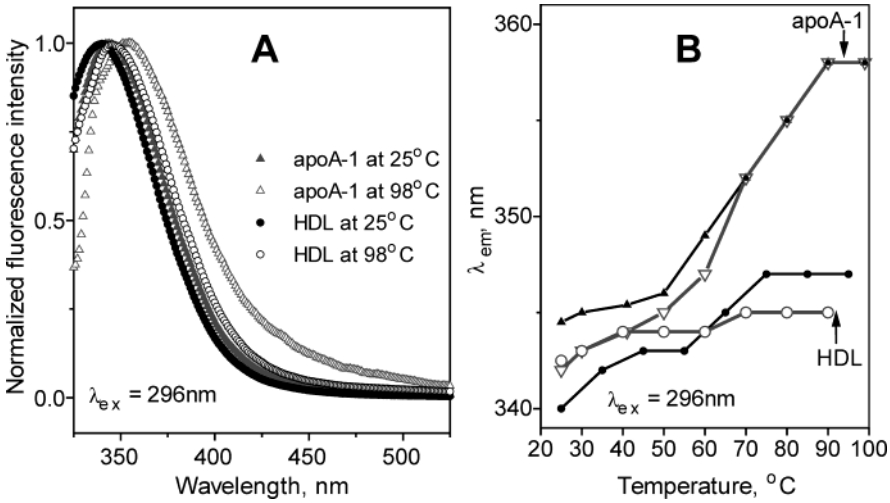

FIGURE 8: Intrinsic Trp fluorescence of HDL and apoA-l at various temperatures. The protein concentration is 10−20 μg/mL, and PEG concentrations are 0−15%. The spectra recorded at different PEG concentrations but otherwise identical conditions fully overlap; therefore, only one spectrum is shown for each condition. (A) Normalized emission spectra: (●) HDL at 25 °C, (○) HDL at 98 °C, (▲) apoA-1 at 25 °C, and (△) apoA-1 at 98 °C. (B) Temperature dependence of the emission wavelength of the maximum Trp fluorescence, λ_{em}: (●) HDL in 0% PEG, (○) HDL in 15% PEG, (▲) apoA-1 in 0% PEG, and (▽) apoA-1 in 15% PEG.

at 98 °C retains the negative CD bands at 208 and 222 nm that are characteristic of an α-helix [Figure 6A (○)], with a substantial molar residue ellipticity at 222 nm [Θ_{222}(98 °C) = −15000 deg cm^2 dmol^{-1}], indicating that HDL proteins retain ∼40% α-helical content at 98 °C. The highly structured state of HDL proteins at high temperatures is also evident from spectroscopic data reported previously (*26*, *41*, *42*). Taken together, these results suggest that in the course of HDL heating to 98 °C apoA-1 dissociates from HDL in a partially lipidated state that prevents the protein from undergoing complete thermal unfolding. The lipidated state of apoA-1 is consistent with the large differences observed between the $\Theta_{222}(T)$ curves of free apoA-1 and the closely superimposing heating and cooling curves of HDL [Figure 6B (triangles and circles)]. Indeed, if a substantial amount of lipid-free apoA-1 dissociated irreversibly from HDL during the first scan to 98 °C, the consecutive scan would represent a weighted average of the first HDL scan and the melting data of lipid-free apoA-1. Thus, the close superimposition of the first scan and consecutive HDL scans indicates that no substantial amount of lipid-free apoA-1 is released when HDL is heated to 98 °C. Consequently, apoA-1 that dissociated from HDL during heating is present in a partially lipidated rather than lipid-free state.

Importantly, our calorimetric and light scattering data show that, during HDL heating at 80−90 °C/h, the conclusion of the first transition in 0% PEG and of the second transition in 15% PEG occurs around 98 °C (Figures 4 and 5, black lines). Consequently, correlation of these data with the far-UV CD melting curves recorded upon heating of HDL in 0−15% PEG to 98 °C [Figure 6B (○ and ●)] indicates that fusion and rupture are not accompanied by any large cooperative α-helical unfolding. This result is consistent with the absence of the scan rate effects or hysteresis in the $\Theta_{222}(T)$ data of HDL (Figure 6B), which is characteristic of a reversible unfolding. This is in stark contrast with the irreversible thermal transitions in HDL detected by DSC, EM, and light scattering (Figures 1, 2, and 5). We conclude that (i) the cooperative irreversible changes in the particle morphology do not involve substantial protein unfolding and thus remain "silent" in far-UV CD and (ii) the gradual heat-induced reduction in the HDL α-helical content reflects the structural "relaxation" that is largely reversed upon cooling [Figure 6B (○ and ●)] rather than cooperative protein unfolding. The absence of any large effects of PEG on the far-UV CD melting curves of HDL [Figure 6B (○ and ●)], which contrasts with large PEG-induced shifts in the DSC curves (Figure 4), can be similarly explained. Indeed, since the calorimetric HDL transitions are not accompanied by significant protein unfolding, the PEG-induced shifts in the $C_p(T)$ data are not paralleled by similar shifts in the $\Theta_{222}(T)$ data.

Like the far-UV CD data, the near-UV CD spectra of HDL at 25 °C [Figure 7A (●)] remain invariant when the PEG concentration is increased from 0 to 15%, indicating the absence of any significant effects of PEG on the aromatic packing in HDL. Comparison of the HDL spectra at 25 and 98 °C shows the largest differences at 270−280 nm [Figure 7A (● and −)], i.e., in the spectral range containing contributions from Tyr and Phe (*43*). These CD differences were utilized to record the near-UV CD melting curves at 270 nm, which maximized the signal-to-noise ratio. Like the $\Theta_{222}(T)$ data in Figure 6B, the $\Theta_{270}(T)$ data recorded during the heating and cooling of HDL largely superimpose, are nearly linear, and are independent of the scan rate or the PEG concentration in the range explored (Figure 7B). This indicates the absence of any cooperative irreversible changes in the aromatic packing upon HDL fusion and rupture. Furthermore, the large discrepancy between the near-UV CD spectrum of lipid-free apoA-1 at 25 °C and the spectra of HDL recorded at 25 °C after heating to 98 °C (compare ▲ and ○ data in Figure 7A) indicates that no significant amount of lipid-free apoA-1 is produced upon HDL fusion and rupture.

To monitor solvent exposure of Trp during the thermal transitions in HDL, intrinsic Trp fluorescence spectra of HDL were recorded at different temperatures and PEG concentrations and were compared with similar spectra of lipid-free apoA-1 (Figure 8). Since apoA-1 is the only major HDL protein that contains Trp, it dominates the intrinsic HDL

fluorescence. Like the far- and near-UV CD spectra, the Trp emission spectra of free apoA-1 and HDL show no significant changes when the PEG concentration is increased from 0 to 15%. Figure 8A shows intrinsic Trp fluorescence spectra of HDL at 25 °C in 0−15% PEG (●). The wavelength of maximal emission, λ_{em}, which was determined from the peak position in these spectra with an accuracy of ±2 nm, ranges from 340 to 343 nm regardless of the PEG concentration [Figure 8B (● and ○)]; this indicates substantial burial of Trp in the apolar environment. A similar but slightly longer λ_{em} is observed for lipid-free apoA-1 in 0−15% PEG at 25 °C [Figure 8A (▲)]. Heating of lipid-free apoA-1 in 0−15% PEG to 98 °C leads to a 14 nm red shift in λ_{em}, from ∼345 nm at 25 °C to 359 nm at 98 °C, indicating complete solvent exposure of Trp in apoA-1 at high temperatures [Figure 8A,B (△)]. In contrast, similar heating of HDL leads to an only ∼5 nm red shift in λ_{em} that does not exceed 347 nm at 98 °C [Figure 8A,B (● and ○)]. This indicates the absence of large changes in the Trp solvent exposure during HDL fusion or rupture. Consequently, consistent with the CD data in Figures 6 and 7, Trp fluorescence data in Figure 8 indicate that the heat-induced HDL fusion and rupture do not involve any large cooperative changes in the Trp solvent exposure, and thus may not involve complete protein delipidation and unfolding.

DISCUSSION

The results of this work suggest that the first calorimetric HDL transition involves not only apoA-1 dissociation but also HDL fusion. This is evident from the electron micrographs showing significant particle enlargement upon heating to the temperature corresponding to the conclusion, but not the onset, of the first calorimetric transition (Figure 2A,B). The changes in the particle size distribution during this thermal transition, which are remarkably similar to those induced by GdmHCl (*17*), show an increased population of the 11−12 nm particles and a reduced population of the 7−9 nm HDL (Figure 3A,B). This suggests fusion of two to three 7−9 nm HDL into one 11−12 nm HDL-like particle, with a possible release of two apoA-1 molecules to compensate for the reduced surface area. A similar fusion reaction is proposed to be involved in the conversion from HDL_3 (d = 7−9 nm) to HDL_2 (d = 11−13 nm) during HDL metabolism (reviewed in refs *4* and *8*). Thus, the products of the heat- or denaturant-induced HDL fusion may resemble those of the enzyme-induced HDL fusion in plasma.

HDL fusion in plasma is subject to tight enzymatic control that is necessary for the correct balance among various HDL subclasses. This suggests that lipoproteins from different subclasses are separated by high energy barriers that slow their unregulated interconversions. The presence of such energy barriers in the heat-induced HDL fusion and rupture is evident from the effects of the heating rate on the transition temperature monitored by light scattering of HDL in 15% PEG (Figure 5). Such scan rate dependence, which was also observed in our heat unfolding studies of reconstituted discoidal HDL (*16*, *18*, *19*), is indicative of irreversible transitions with a high activation energy (enthalpy) (*40*). Earlier, we proposed that the general physical origin of this activation energy is the transient disruption of the protein and/or lipid packing interactions during morphological transitions, such as heat-induced fusion of discoidal HDL

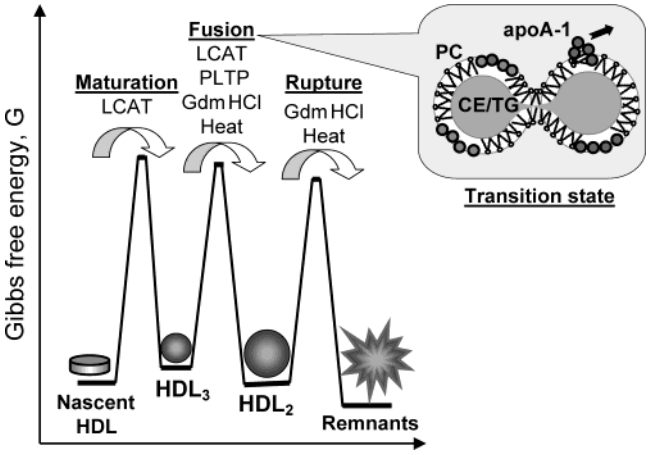

FIGURE 9: Free energy profile for HDL interconversions. Local free energy minima corresponding to different HDL subclasses are separated by high energy barriers ($\Delta G^* \cong 16-17$ kcal/mol) that confer HDL stability and slow their spontaneous interconversions (*16*, *17*). These barriers can be overcome by plasma enzymes such as LCAT, PLTP, or CETP and/or by denaturing agents. Observation of comparable free energy barriers for PEG-mediated liposome fusion and rupture (*32*) suggests that the transition states in HDL fusion and rupture resemble aspects of the transition states in membrane, secretory, and viral fusion. The cartoon on the right shows the putative high-energy transition state in HDL fusion accompanied by dissociation of lipid-poor apoA-1; protein α-helices on the particle surface are shown as circles. Such a fusion reaction can be induced by plasma factors [LCAT, PLTP, CETP, or hepatic lipase (*4*, *8*)], by GdmHCl (*17*), or by heating (this work).

(*16*, *18*, *19*) or GdmHCl-induced fusion and rupture of spherical HDL (*17*). The data in Figure 5 support this hypothesis and indicate that the heat-induced fusion and rupture of spherical HDL are also associated with a high activation energy and thus are subject to kinetic control.

Our results suggest that not only the products and the kinetic character but also the structural basis for the heat-, denaturant-, and enzyme-induced HDL fusion may be similar. Indeed, HDL fusion in our studies is probably triggered by an imbalance between the protein-depleted particle surface and the apolar core, which results from the protein unfolding and/or dissociation from the surface. The LCAT reaction may create a similar imbalance by increasing the level of core CE at the expense of the surface cholesterol and PC (*4*, *8*−*10*); in addition, the phospholipase activity of LCAT generates lysoPC that promotes fusion (*27*). Similarly, PLTP-induced fusion of apoA-1-deficient HDL has been proposed to be triggered by the PLTP-mediated proteolysis and displacement of apoA-1 (*44*). Fusion of apoA-1-depleted HDL has also been observed in other studies (*45*, *46*). Taken together, these results indicate that HDL fusion can be triggered by an imbalance between the particle surface and its core resulting from the surface depletion of the polar protein or lipid moiety (which occurs in the heat-, denaturant-, PLTP-, and LCAT-induced fusion) and/or from an increase in the apolar lipid core (in LCAT-induced fusion) (Figure 9).

The proposed mechanism of HDL fusion implies that apoA-1 on HDL is an important fusion inhibitor. Indeed, in the absence of apolipoproteins such as apoA-1, HDL disks and spheres are unstable and fuse to form larger lipid particles. In addition to maintaining the particle integrity, the fusion inhibitory activity of apoA-1 may also be essential

in the selective uptake of CE from HDL by the hepatic HDL receptor, scavenger receptor BI (SR-BI) (*47*). Indeed, the interaction of apoA-1 with SR-BI has been reported to prevent fusion of the lipid donor with the plasma membrane, thereby allowing selective uptake of CE (*48*), which is a crucial step in reverse cholesterol transport. The fusion inhibitory activity of apoA-1 and its lipid-binding fragments has also been reported to account for their antiviral properties (*49*). Furthermore, apoA-1 has been shown to inhibit the fusion of LDL with CE microemulsions (*50*) and to prevent phospholipase C-induced LDL aggregation and fusion (*51*). Taken together, these results suggest that inhibition of lipoprotein fusion constitutes an essential physiological function of apoA-1.

The results of this work indicate that the apoA-1 that dissociates from HDL during the heat-induced fusion is lipidated. This is evident from the comparison of the far- and near-UV CD and fluorescence data recorded from HDL and lipid-free apoA-1 in 0−15% PEG at 10−98 °C (Figures 6−8). However, the observation of the DSC peak reflecting the unfolding of the dissociated apoA-1 at 58 °C (curves 3 and 4 in Figure 1), which is the melting temperature of lipid-free apoA-1 (*39* and references therein), along with the earlier DSC and centrifugation data (*36*−*38*), suggests that the apoA-1 dissociated from the thermally fused HDL contains only a small amount of lipid and thus can be considered lipid-poor. Similarly, our spectroscopic studies of model discoidal HDL containing human apoC-1 showed that the heat-induced unfolding and disk fusion do not involve complete protein delipidation (*16*). Our current results confirm this conclusion and extend it toward spherical HDL. Although the lipidation level of apoA-1 dissociated from HDL during metabolic events such as enzyme-induced fusion is difficult to determine in detail (*11*), apoA-1 is generally characterized as lipid-poor. Such monomolecular lipid-poor forms of apoA-1 have recently become a focus of intense investigation, since they are particularly effective at promoting cellular cholesterol efflux due to their interaction with an ATP-binding cassette protein on the cell surface (reviewed in refs *11*, *50*, and *53*). It is possible that apoA-1 dissociates from the thermally fused HDL in a similar lipid-poor form.

The lipid-poor state of apoA-1 released from the thermally fused HDL prevents the protein from complete unfolding at 98 °C upon heat-induced fusion and rupture of HDL (Figure 6). The absence of such unfolding is consistent with the near-UV CD and fluorescence data of HDL (Figures 7 and 8), and with the spectroscopic data from other groups (*26*, *41*, *42*). This result contrasts with the complete protein unfolding observed upon GdmHCl denaturation of spherical plasma HDL (*17*). This difference suggests that, in contrast to lipid-poor apoA-1 released during the heat-induced fusion of spherical HDL, the apoA-1 released during GdmHCl-induced fusion and rupture of spherical HDL may be lipid-free. The absence of substantial protein unfolding in the heat-induced HDL fusion and rupture indicates that the heat effects of these endothermic transitions originate from lipid and/or protein dissociation rather than from protein unfolding. This is consistent with the narrow peak width of the two calorimetric transitions (Figures 1 and 4) that is characteristic of lipid repacking rather than apolipoprotein unfolding.

An unexpected result is the observation of the PEG-induced increase in the particle diameter at 22 °C. This reaction is different from the heat-, denaturant-, or enzyme-induced HDL fusion, since it leads to formation of larger, more heterogeneous particles (Figure 3C) and does not involve apoA-1 dissociation; the latter is indicated by the absence of the peak at 58 °C in the DSC data of the PEG-fused HDL (Figure 4). Thus, despite substantial reduction in the combined surface area, the PEG-fused particles accommodate the same proportion of protein as intact HDL. One possibility is that PEG induces subtle conformational changes in apoA-1 that reduce the protein−lipid contact area and thereby help to accommodate the protein at the particle surface; similar changes may be involved in HDL fusion by plasma enzymes (such as phospholipase A2) that does not involve apoA-1 dissociation (*54*). However, no such PEG-induced conformational changes in HDL proteins were detected in our studies (Figures 6−8). Alternatively, PEG may increase the fluidity of the highly curved PC monolayer on the HDL surface, thereby aiding accommodation of the excess protein. Regardless of the mechanism, the observation of the PEG-induced HDL fusion illustrates the potential for more than one possible mode of lipoprotein fusion.

HDL fusion at 22 °C caused by 7.5 and 15% PEG-8000 was surprising since similar PEG concentrations promote liposome fusion but do not trigger it in the absence of additional perturbations (*30*−*33*). Thus, PEG appears to be more effective in mediating fusion of HDL than liposomes. One possible explanation is that the transition state in HDL fusion involves deformation of the PC monolayer (Figure 9), whereas liposome fusion involves deformation of the lipid bilayer which may be more energetically costly. The difference in the lipid packing on the surface of highly curved HDL and of much larger lipid vesicles may also be a factor. In summary, our results show that PEG-8000 is a potent HDL fusogen.

Interestingly, the large PEG-induced increase in the particle size has relatively little effect on the apparent thermal stability of HDL. Indeed, HDL incubated in 15% PEG and dialyzed against the PEG-free buffer show only a small −4 °C shift in the apparent transition temperatures compared to that of intact HDL (DSC data not shown). In contrast, the presence of 15% PEG in the HDL solution during heating leads to a much larger shift of −18 °C in the DSC peaks (Figure 4). Consequently, the presence of PEG in solution leads to low-temperature shifts in the HDL fusion and rupture transitions, and thereby reduces the thermal stability of HDL. Thus, consistent with our hypothesis, fusogenic concentrations of PEG induce HDL fusion and destabilization.

The absence of significant effects of PEG on the apoA-1 conformation or thermal stability revealed by the spectroscopic data in Figures 6−8 suggests that the PEG-induced HDL destabilization results from the effects of PEG on the lipid rather than the protein moiety. Thus, HDL stability can be affected not only by protein denaturants such as GdmHCl but also by lipid fusogens such as PEG. The utility of PEG-8000 for the analysis of HDL transitions is evident from the large reduction in the transition temperatures in 15% PEG (Figure 4), which facilitates the spectroscopic observation not only of the heat-induced HDL fusion but also of HDL rupture below 100 °C (Figures 5−8). PEG-8000 has been widely used for the detailed analysis of the molecular events involved in membrane, viral, and secretory fusion (*27*−*33*). The results reported here suggest that PEG may also be useful

for the analyses of molecular events involved in HDL fusion and rupture. Our results also caution against using PEG for lipoprotein isolation (*55*, *56*).

In summary, this study demonstrates, for the first time, that (i) the first calorimetric transition in HDL involves particle fusion, (ii) heat-induced HDL fusion and rupture are kinetically controlled, (iii) in contrast to the GdmHCl-induced HDL transitions, the heat-induced HDL fusion and rupture do not involve complete apolipoprotein unfolding and delipidation, (iv) PEG-8000 induces HDL fusion at 22 °C that is different from the heat- or denaturant-induced fusion, and (v) PEG-8000 does not affect the structure or stability of lipid-free apoA-1 but destabilizes HDL and leads to a large reduction in the transition temperatures without significantly altering the nature of these transitions. Therefore, PEG-8000 may provide a useful model agent for the analysis of molecular events involved in HDL remodeling and fusion by plasma factors.

ACKNOWLEDGMENT

We thank Cheryl England and Michael Gigliotti for lipoprotein and apolipoprotein isolation and purification and Sangeeta Benjwal for her help with many experiments. We are grateful to Dr. R. Andrew Zoeller who generously allowed us to use his Fluoromax-2 fluorimeter.

REFERENCES

1. Eisenberg, S. (1990) Metabolism of apolipoproteins and lipoproteins, *Curr. Opin. Lipidol. 1*, 205−215.
2. Atkinson, D., and Small, D. M. (1986) Recombinant lipoproteins: implications for structure and assembly of native lipoproteins, *Annu. Rev. Biophys. Biophys. Chem. 15*, 403−456.
3. Lund-Katz, S., Liu, L., Thuahnai, S. T., and Phillips, M. C. (2003) High-density lipoprotein structure, *Front. Biosci. 8*, d1044−d1054.
4. Rye, K. A., Clay, M. A., and Barter, P. J. (1999) Remodeling of high-density lipoproteins by plasma factors, *Atherosclerosis 145* (2), 227−238.
5. Mackness, M. I., and Durrington, P. N. (1995) HDL, its enzymes and its potential to influence lipid peroxidation, *Atherosclerosis 115* (2), 243−253.
6. Gordon, T., Castelli, W. P., Hjortland, M. C., Kannel, W. B., and Dawber, T. R. (1977) High-density lipoproteins as a protective factor against coronary heart disease. The Framingham study, *Am. J. Med. 62*, 707−714.
7. Duriez, P., and Fruchart, J. C. (1999) High-density lipoprotein subclasses and apolipoprotein A-I, *Clin. Chim. Acta 286* (1−2), 97−114.
8. Barter, P. J. (2002) Hugh Sinclair Lecture: The regulation and remodeling of HDL by plasma factors, *Atheroscler. Suppl. 3* (4), 39−47.
9. Nichols, A. V., Blanche, P. J., Gong, E. L., Shore, V. G., and Forte, T. M. (1985) Molecular pathways in the transformation of model discoidal lipoprotein complexes induced by lecithin: cholesterol acyltransferase, *Biochim. Biophys. Acta 834* (3), 285−300.
10. Clay, M. A., Pyle, D. H., Rye, K. A., and Barter, P. J. (2000) Formation of spherical, reconstituted high-density lipoproteins containing both apolipoproteins A-I and A-II is mediated by lecithin:cholesterol acyltransferase, *J. Biol. Chem. 275* (12), 9019−9025.
11. Rye, K. A., and Barter, P. J. (2004) Formation and metabolism of prebeta-migrating, lipid-poor apolipoprotein A-I, *Arterioscler. Thromb. Vasc. Biol. 24* (3), 421−428.
12. Lusa, S., Jauhiainen, M., Metso, J., Somerharju, P., and Ehnholm, C. (1996) The mechanism of human plasma phospholipid transfer protein-induced enlargement of high-density lipoprotein particles: evidence for particle fusion, *Biochem. J. 313* (Part 1), 275−282.
13. Korhonen, A., Jauhiainen, M., Ehnholm, C., Kovanen, P. T., and Ala-Korpela, M. (1998) Remodeling of HDL by phospholipid transfer protein: demonstration of particle fusion by ^{1}H NMR spectroscopy, *Biochem, Biophys. Res. Commun. 9* (3), 910−916.
14. Settasatian, N., Duong, M., Curtiss, L. K., Ehnholm, C., Jauhiainen, M., Huuskonen, J., and Rye, K. A. (2001) The mechanism of the remodeling of high-density lipoproteins by phospholipid transfer protein, *J. Biol. Chem. 276* (29), 26898−26905.
15. Rye, K. A., Hime, N. J., and Barter, P. J. (1997) Evidence that cholesteryl ester transfer protein-mediated reductions in reconstituted high-density lipoprotein size involve particle fusion, *J. Biol. Chem. 272* (7), 3953−3960.
16. Gursky, O., Ranjana, and Gantz, D. L. (2002) Complex of human apolipoprotein C-1 with phospholipid: thermodynamic or kinetic stability? *Biochemistry 41* (23), 7373−7384.
17. Mehta, R., Gantz, D. L., and Gursky, O. (2003) Human plasma high-density lipoproteins are stabilized by kinetic factors, *J. Mol. Biol. 328* (1), 183−192.
18. Mehta, R., Gantz, D. L., and Gursky, O. (2003) Effects of mutations in apolipoprotein C-1 on the reconstitution and kinetic stability of discoidal lipoproteins, *Biochemistry 42* (16), 4751−4758.
19. Fang, Y., Gursky, O., and Atkinson, D. (2003) Lipid-Binding studies of human apolipoprotein A-I and its terminally truncated mutants, *Biochemistry 42* (45), 13260−13268.
20. Reijngoud, D. J., and Phillips, M. C. (1982) Mechanism of dissociation of human apolipoprotein A-I from complexes with dimyristoylphosphatidylcholine as studied by guanidine hydrochloride denaturation, *Biochemistry 21* (12), 2969−2976.
21. Epand, R. M. (1982) The apparent preferential interaction of human plasma high-density apolipoprotein A-I with gel-state phospholipids, *Biochim. Biophys. Acta 712* (1), 146−151.
22. Surewicz, W. K., Epand, R. M., Pownall, H. J., and Hui, S. W. (1986) Human apolipoprotein A-I forms thermally stable complexes with anionic but not with zwitterionic phospholipids, *J. Biol. Chem. 261* (34), 16191−16197.
23. Nichols, A. V., Gong, E. L., Blanche, P. J., Forte, T. M., and Anderson, D. W. (1976) Effects of guanidine hydrochloride on human plasma high-density lipoproteins, *Biochim. Biophys. Acta 446* (1), 226−239.
24. Tall, A. R., and Small, D. M. (1977) Solubilization of phospholipid membranes by human plasma high-density lipoproteins, *Nature 265* (5590), 163−164.
25. Rosseneu, M., Van Tornout, P., Lievens, M. J., Schmitz, G., and Assmann, G. (1982) Dissociation of apolipoprotein AI from apoprotein−lipid complexes and from high-density lipoproteins. A fluorescence study, *Eur. J. Biochem. 128* (2−3), 455−460.
26. Gwynne, J., Brewer, H. B., Jr., and Edelhoch, H. (1975) The molecular behavior of apoA-I in human high-density lipoproteins, *J. Biol. Chem. 250* (6), 2269−2274.
27. Blumenthal, R., Clague, M. J., Durell, S. R., and Epand, R. M. (2003) Membrane fusion, *Chem. Rev. 103* (1), 53−69.
28. MacDonald, R. I. (1985) Membrane fusion due to dehydration by polyethylene glycol, dextran, or sucrose, *Biochemistry 24* (15), 4058−4066.
29. Hermann, A., Clague, M. J., and Blumenthal, R. (1993) Enhancement of viral fusion by non-adsorbing polymers, *Biophys. J. 65* (1), 528−534.
30. Lentz, B. R., McIntyre, G. F., Parks, D. J., Yates, J. C., and Massenburg, D. (1992) Bilayer curvature and certain amphipaths promote poly(ethylene glycol)-induced fusion of dipalmitoyl phosphatidylcholine unilamellar vesicles, *Biochemistry 31* (10), 2643−2653.
31. Lentz, B. R. (1994) Polymer-induced membrane fusion: potential mechanism and relation to cell fusion events, *Chem. Phys. Lipids 73* (1−2), 91−106.
32. Lee, J., and Lentz, B. R. (1998) Secretory and viral fusion may share mechanistic events with fusion between curved lipid bilayers, *Proc. Natl. Acad. Sci. U.S.A. 95* (16), 9274−9279.
33. Haque, M. E., and Lentz, B. R. (2002) Influence of gp41 fusion peptide on the kinetics of poly(ethylene glycol)-mediated model membrane fusion, *Biochemistry 41* (35), 10866−10876.
34. Schumaker, V. N., and Puppione, D. L. (1986) Sequential flotation ultracentrifugation, *Methods Enzymol. 128*, 155−170.
35. Wetterau, J. R., and Jonas, A. (1982) Effect of dipalmitoylphosphatidylcholine vesicle curvature on the reaction with human apolipoprotein A-I, *J. Biol. Chem. 257* (18), 10961−10966.
36. Tall, A. R., Deckelbaum, R. J., Small, D. M., and Shipley, G. G. (1977) Thermal behavior of human plasma high-density lipoprotein, *Biochim. Biophys. Acta 487* (1), 145−153.

37. Tall, A. R., Puppione, D. L., Kunitake, S. T., Atkinson, D., Small, D. M., and Waugh, D. (1981) Organization of the core lipids of high-density lipoproteins in the lactating bovine, *J. Biol. Chem. 256* (1), 170−174.
38. Tall, A. R., and Green, P. H. (1981) Incorporation of phosphatidylcholine into spherical and discoidal lipoproteins during incubation of egg phosphatidylcholine vesicles with isolated high-density lipoproteins or with plasma, *J. Biol. Chem. 256* (4), 2035−2044.
39. Gursky, O., and Atkinson, D. (1996) Thermal unfolding of human high-density apolipoprotein A-1: implications for a lipid-free molten globular state, *Proc. Natl. Acad. Sci. U.S.A. 93* (7), 2991−2995.
40. Sanchez-Ruiz, J. M. (1992) Theoretical analysis of Lumry-Eyring model in differential scanning calorimetry, *Biophys. J. 61*, 921−935.
41. Scanu, A. M. (1969) On the temperature dependence of the conformation of human serum high-density lipoprotein, *Biochim. Biophys. Acta 181* (1), 268−274.
42. Leslie, R. B. (1971) Some physical and physico-chemical approaches to the structure of serum high-density lipoproteins (HDL), *Biochem. Soc. Symp. 33*, 47−85.
43. Woody, R. W., and Dunker, A. K. (1996) Aromatic and cysteine side-chain circular dichroism in proteins, in *Circular Dichroism and Conformational Analysis of Biomolecules* (Fasman, G. D., Ed.) pp 110−157, Plenum Press, New York.
44. Nishida, H. I., Klock, D. G., Guo, Z., Jakstys, B. P., and Nishida, T. (1997) Phospholipid transfer protein can transform reconstituted discoidal HDL into vesicular structures, *Biochim. Biophys. Acta 1349* (3), 222−232.
45. Tall, A. R., and Small, D. M. (1977) Solubilization of phospholipid membranes by human plasma high-density lipoproteins, *Nature 265* (5590), 163−164.
46. Tall, A. R., Hogan, V., Askinazi, L., and Small, D. M. (1978) Interaction of plasma high-density lipoproteins with dimyristoylllecithin multilamellar liposomes, *Biochemistry 17*, 322−326.
47. Acton, S., Rigotti, A., Landschulz, K. T., Xu, S., Hobbs, H. H., and Krieger, M. (1996) Identification of scavenger receptor SR-BI as a high-density lipoprotein receptor, *Science 271* (5248), 518−520.
48. Thuahnai, S. T., Lund-Katz, S., Williams, D. L., and Phillips, M. C. (2001) Scavenger receptor class B, type I-mediated uptake of various lipids into cells. Influence of the nature of the donor particle interaction with the receptor, *J. Biol. Chem. 276* (47), 43801−43808.
49. Srinivas, R. V., Venkatachalapathi, Y. V., Rui, Z., Owens, R. J., Gupta, K. B., Srinivas, S. K., Anantharamaiah, G. M., Segrest, J. P., and Compans, R. W. (1991) Inhibition of virus-induced cell fusion by apolipoprotein A-I and its amphipathic peptide analogs, *J. Cell. Biochem. 45* (2), 224−237.
50. Yancey, P. G., Bortnick, A. E., Kellner-Weibel, G., De La Llera-Moya, M., Phillips, M. C., and Rothblat, G. H. (2003) Importance of Different Pathways of Cellular Cholesterol Efflux, *Arterioscler. Thromb. Vasc. Biol. 23* (5), 712−719.
51. Parks, J. S., Martin, J. A., Johnson, F. L., and Rudel, L. L. (1985) Fusion of low-density lipoproteins with cholesterol ester-phospholipid microemulsions. Prevention of particle fusion by apolipoprotein A-I, *J. Biol. Chem. 260* (5), 3155−3163.
52. Liu, H., Scraba, D. G., and Ryan, R. O. (1993) Prevention of phospholipase-C induced aggregation of low-density lipoprotein by amphipathic apolipoproteins, *FEBS Lett. 316* (1), 27−33.
53. Oram, J. F. (2002) ATP-binding cassette transporter A1 and cholesterol trafficking, *Curr. Opin. Lipidol. 13* (4), 373−381.
54. Rye, K. A., and Duong, M. N. (2000) Influence of phospholipid depletion on the size, structure, and remodeling of reconstituted high-density lipoproteins, *J. Lipid Res. 41* (10), 1640−1650.
55. Lippi, U., Graziani, M. S., Manzato, F., and Schinella, M. (1987) Procedure for effective separation of high-density lipoproteins in normal serum and hypertriglyceridemic samples, *Clin. Biochem. 20* (5), 313−315.
56. Leino, A., Viikari, J., Koskinen, P., and Irjala, K. (1987) Problems with PEG-based precipitation methods in the determination of HDL2- and HDL3-cholesterol, *Scand. J. Clin. Lab. Invest. 47* (7), 705−708.

BI036274R